α,1,6-Fucosyltransferase (FUT8) regulates cancer-promoting capacities of cancer-associated fibroblasts (CAFs) through the modification of EGFR core fucosylation in non-small cell lung cancer

Fengzhou Li
First Affiliated Hospital of Dalian Medical University
Shilei Zhao
First Affiliated Hospital of Dalian Medical University
Yanwei Cui
Affiliated Zhongshan Hospital of Dalian University
Jiaqi Qiang
Dalian Municipal Central Hospital Affiliated of Dalian Medical University
Tao Guo
First Affiliated Hospital of Dalian Medical University
Wei Sun
Peking Union Medical College Hospital
Zhe Sun
First Affiliated Hospital of Dalian Medical University
Zhuoshi Li
First Affiliated Hospital of Dalian Medical University
Lei Fang
First Affiliated Hospital of Dalian Medical University
Qiang Xie
First Affiliated Hospital of Dalian Medical University
Wendan Yu
Dalian Medical University
Wei Guo
Dalian Medical University
Chundong Gu (guchundong@dmu.edu.cn)
First Affiliated Hospital of Dalian Medical University
Wuguo Deng
Sun Yat-sen University Cancer Center
Taihua Wu (wutaihuadoc@126.com)
First Affiliated Hospital of Dalian Medical University https://orcid.org/0000-0001-9544-818X

Research

Keywords: bioinformatics, fibroblasts, CAF, cancer-associated fibroblasts, FUT8, lung cancer

Posted Date: December 12th, 2019

DOI: https://doi.org/10.21203/rs.2.18620/v1

Abstract

Background

Cancer-associated fibroblasts (CAFs), the main component of the tumor microenvironment (TME) of NSCLC, are activated by phenotypic transformation into myofibroblasts. α,1,6-fucosyltransferase (FUT8), the key enzyme catalyzing core α,1,6-fucosylation (CF), plays important roles in multiple malignancies. In the current study, we investigated the functions and mechanism of CF mediated by FUT8 in CAFs in NSCLC through bioinformatics analysis, retrospective clinical studies and in vitro/in vivo laboratory experiments.

Methods

Bioinformatics was used to reveal the relationship between FUT8 and CAFs. Resected specimens, clinical data and prognostic information from 135 NSCLC patients were analyzed to assess the prognostic value of FUT8 in CAFs. Primary CAFs and normal lung fibroblasts were extracted from NSCLC patients and cocultured with NSCLC cell lines in a novel noncontact coculture device produced by 3D printing. In vivo, CAF/NSCLC coinjection tumorigenesis assay was performed in nude mice to study the function of FUT8/CF in TME. The mechanisms of FUT8/CF in CAFs regulating the cocultured NSCLC cells were investigated in cell and molecular experiments.

Results

FUT8 in CAFs is an independent risk factor for prognosis. FUT8/CF in CAFs is essential for CAFs to maintain their ability to promote NSCLC. FUT8/CF in CAFs is responsible for the cancer-promoting capacities of CAFs and lead to a malignant tumor microenvironment. CF modification enhances tyrosine phosphorylation of EGFR in CAFs, which causes activation of downstream signalings of EGFR and maintains cancer-promoting properties of CAFs.

Conclusion

FUT8 regulates cancer-promoting capacities of CAFs via the modification of EGFR CF in non-small cell lung cancer.

1. Background

Lung cancer is the most common malignancy in the world[1], and non-small cell lung cancer (NSCLC) accounts for approximately 85% of lung cancer cases[2]. Despite advances in the diagnosis and treatment of lung cancer, the five-year survival rate is still below 30%[3]. Due to the presence of micrometastasis, even early-stage patients are at risk of metastasis and relapse after radical treatment[4]. Therefore, the mechanism of NSCLC proliferation and metastasis still needs to be further explored, and

more accurate prognostic indicators and more effective molecular therapeutic targets need to be identified.

In recent years, crosstalk between the tumor microenvironment (TME) and cancer cells has received increasing attention[5]. The TME is the internal environment in which cancer cells grow in association with “nontumoral” components[6]. Cancer-associated fibroblasts (CAFs), the main component of the TME of NSCLC, account for 70% of the cells in solid tumors[7] and are most often identified by the expression of specific biomarkers such as α-smooth muscle actin (α-SMA) [8], fibroblast activating protein (FAP) and vimentin[9]. CAFs can promote tumor progression through direct interaction and the secretion of various cytokines[10]. Major studies have demonstrated that CAFs are transformed from normal lung fibroblasts to a myofibroblast phenotype and then acquire cancer-associated properties. Thus, elucidation of the mechanisms of the activation and maintenance of CAFs could lead to novel diagnostic and therapeutic approaches.

Glycosylation is a common type of posttranslational modification of proteins. It is important for the folding, stability, and many of the biologic functions of glycoproteins[11]. Glycosylation can be divided into O-linked glycosylation and N-linked glycosylation according to the position of the sugar modification, and the latter is more common[12]. Fucosylation catalyzed by fucosyltransferases is one of the most common forms of glycosylation [13]. Among the 13 fucosyltransferases known to be encoded by the human genome[14], α,1,6-fucosyltransferase(FUT8), which is also known as α1,6-fucosyltransferase, is the only enzyme that catalyzes the core α1,6-fucosylation of asparagine-linked oligosaccharides in mammals[15]. FUT8 is responsible for the transfer of a fucosyl moiety from guanosine diphosphate (GDP)-fucose to the innermost GlcNAc residue of hybrid and complex asparagine-linked oligosaccharides in glycoproteins via α1,6 linkage to generate the core fucosylation (CF) [16].This modification was essential for the development and progression of cancer[11, 14, 17–20], including NSCLC. However, whether FUT8/CF plays an important role in the TME remains unknown.

Epidermal growth factor receptor (EGFR), a member of the ERBB family of receptor tyrosine kinase super-family of cell surface receptors, have received much attention given their strong association with malignant proliferation[21]. EGFR serves as a mediator of cell signaling by extra-cellular growth factors to activate intracellular pathways such as PI3K/AKT/mTOR, JAK/STAT and MAPK/ERK[22]. Deregulation of EGFR signaling is also common in CAFs[23–25]. It was reported that the modification of EGFR fucosylation is essential for the activation of EGFR by tyrosine phosphorylation [26–28]. Extracellular ligands of EGFR such as epidermal growth factor (EGF)[29, 30], transforming growth factor -alpha (TGF-α)[31], neuregulin1 (NRG1)[32] and G protein estrogen receptor (GPER)[23] were identified to be essential for the activation and maintenance of CAFs. Moreover, EGFR signaling were reported to be important for the cancer-promoting ability of CAFs in breast cancer[23]. However, whether CF mediated by FUT8 regulates the cancer-promoting ability of CAFs in NSCLC is not elucidated.

Our previous study showed that FUT8/CF is involved in the transformation of pericytes and fibroblasts into myofibroblasts in pulmonary fibrosis[33], which is very similar to the process in which normal lung fibroblasts are activated to become CAFs. Therefore, we begin with the hypothesis that FUT8/CF in CAFs plays a key role in the activation and maintenance of the cancer-promoting capacities of CAFs in NSCLC. During the study, we found that the activity of the ERBB family and its downstream signaling pathways in CAFs was regulated by FUT8, and further, we identified EGFR as a key protein that was regulated by FUT8/CF. Subsequently, we confirmed the effect of FUT8 by regulating the activity EGFR on CAFs' cancer-promoting capacities through molecular and cell biology experiments. yIn addition, we aimed to explore whether the FUT8/CF levels in the TME serve as a prognostic indicator or potential therapeutic target for NSCLC.

2. Materials And Methods

2.1 Oncomine database

To understand the correlation between FUT8 and lung cancer, we carried out data mining of the gene expression database of lung cancer samples of Oncomine (https://www.oncomine.org/), which is the world's largest gene chip database and integrated data mining platform. The datasets were searched with the filters as follows: □ Gene: FUT8□□ Analysis: Cancer vs. Normal Analysis;□ Cancer type: Lung Cancer; □ Data Type: mRNA or DNA copy number; □ p-value: 0.05; □ Fold Change: 1.5; □ Gene Rank: 10%. The method of data analysis is based on previous published articles[34-36]. Box charts were drawn to show the expression of FUT8 in each dataset. The t-test was used to assess the differences between groups.

2.2 Patient characteristics and tissue preparation

Specimens from 135 patients (median age: 64 years; range 30-82) who underwent complete resection of lung adenocarcinomas were consecutively obtained at the First Affiliated Hospital of Dalian Medical University during January 2013 and December 2014. None of the patients received chemotherapy or radiotherapy prior to the operation. *The 8th Edition International Union Against Cancer/American Joint Committee on Cancer TNM classification*[37] was applied to all enrolled patients. Baseline data and clinicopathological information were collected from the medical record system (Dr. Fengzhou Li & Dr. Zhuoshi Li). Postoperative follow-up was completed by outpatient follow-up and telephone interviews (Dr. Fengzhou Li & Dr. Zhe Sun). The total follow-up period was 61 months, and any patient who was lost to follow-up or died of causes other than lung cancer was recorded as censored at the time of the most recent follow-up. The study was approved by the Medical Ethical Committees of the First Hospital of Dalian Medical University. All specimens were obtained from primary lesions, fixed with formalin, embedded with paraffins, and continuously sliced at a thickness of 4 μm.

2.3 Immunohistochemistry staining and evaluation of expression level

IHC staining for FUT8 and α-SMA was performed according to the manufacturer's instructions of the products used in our previous studies[38, 39]. A streptavidin–peroxidase staining kit was purchased from

ZSGB (Beijing, China) BIO. The paraffin-embedded tissues were dewaxed and rehydrated. The tissues were incubated with primary antibodies diluted to the recommended concentration overnight at 4°C. 3,3'-diaminobenzidine (DAB) staining was performed, and the results were observed under a microscope. Pathological diagnosis was performed according to the 2015 World Health Organization classification of lung tumors[40] and the International Association for the Study of Lung Cancer/ American Thoracic Society/European Respiratory Society International multidisciplinary classification of lung adenocarcinoma[41]. The evaluation of expression was conducted by three professional pathologists separately (Dr. Ling Song, Mr. Sheng Hu and Dr. Jiaqi Qiang). Any dispute was settled by majority rule. The sites and extents of the tumor stroma (mainly consisting of CAFs) were clearly marked by α-SMA staining. In another slice of the same tissue, the expression levels of FUT8 in CAFs were then evaluated according to the methodologies indicated in previous reports for evaluating protein levels in CAFs[42-46].

2.4 Culture of primary fibroblasts

Tissue samples from 9 patients with a definitive p-stage IIIA~IIIB NSCLC were collected at the First Affiliated Hospital of Dalian Medical University from February to May in 2018. The tissues were resected and soaked in DMEM at 0℃ and digested within 2 h in the lab. Tumor tissues and paired normal lung tissues (collected 4~5 cm from the incisal margin) were homogenized and digested for 2.5~4 h at 37℃ in DMEM containing 0.1 mg/mL Roche DNase I (Basel, Switzerland) and 1 mg/mL Roche collagenase A. The cells were filtered with a 75 μm filter and then resuspended and plated with DMEM containing 1% penicillin/streptomycin and 15% GIBCO fetal bovine serum (FBS, Massachusetts, US). The cultures were maintained at 37℃ in 5% CO_2. After 5 passages, cell purity was tested by RT-PCR. In general, primary fibroblasts extracted in this way can survive for 10 to 14 consecutive passages in vitro. Then, CAFs were immortalized with the SV40-large T antigen (EX-SV40T-Lv105, GeneCopoeia/Funeng, Guangdong Province, China) following the recommended protocol. Finally, 5 paired primary fibroblast cell lines were successfully extracted and cultured and were subsequently cultured in DMEM containing 1% penicillin/streptomycin and 10% FBS.

2.5 Cell lines and in vitro cell culture

We selected cell lines for in vitro experiments that could grow in the same medium (Dulbecco's modified eagle medium, DMEM) to observe their interaction in the coculture system. The human NSCLC cell lines A549 and H322 were obtained from the American Type Culture Collection (ATCC, Virginia, US). The human lung fibroblast cell lines HLF, MRC5 and HFL1 were gifts from the Institute of Cancer Stem Cells of Dalian Medical University. All the cell lines were cultured in DMEM containing 1% penicillin/streptomycin and 10% FBS at 37°C under 5% CO_2.

2.6 Noncontact coculture system

A noncontact coculture device was designed (already in the patent examination and approval process in China) and generated by 3D printing (Wanwan 3D, Guangdong Province, China) with highly transparent

nontoxic resin to simulate the internal environment. The reliability of the device was verified in our recent studies[47]. The schematic diagram of the device used for 3D printing is shown in Figure 3C, and a modified version that was easier to produce was used in this study (Figure 3D). The device was a vessel consisting of two culture wells and a precipitation well. The culture wells and the precipitation well were separated by two 2 mm-high partitions. The efficiency of solute exchange was tested with a standard protein solution by measuring the relationship between concentration changes and time in the two culture wells.

During cell seeding, the levels of the liquid in both culture wells should be kept below the height of the partition. Fibroblasts and NSCLC cells were seeded into the two culture wells, at a 2:1 ratio. After cell adherence, DMEM containing 10% FBS was added to the vessel until the level was above the partition. Based on the design of the coculture device, floating cells do not go directly into the contralateral culture well but are deposited into the precipitation well. Before the cells were manipulated in any way, the medium in the precipitation well was drained in case any floating cells had entered the contralateral culture well. Then, the two cell lines were isolated again, and 0.5% trypsin was used for the separate passage/collection of the two cell lines.

2.7 Conditioned medium

Fibroblasts were cultured in DMEM with 10% FBS and routine antibiotics. The medium was changed to FBS-free medium when the cells had reached 80% confluence. After 48 h, the supernatant was extracted and centrifuged at 1600×g for 10 min. The conditioned medium (CM) was stored at –79°C and used for the colony formation assay.

2.8 Reagents and antibodies

Primary antibodies against α-SMA and FUT8 were purchased from Abcam (Cambridge, UK). Primary antibodies against EGFR, β-actin and ST6Gal1 were purchased from Proteintech (Hubei Province, China). Primary antibodies against p-EGFR was purchased from Santa Cruz (Texas, USA), A primary antibody against Twist was purchased from Wanleibio (Liaoning Province, China). Primary antibody kits for EMT markers (9782, against N-cadherin, vimentin, Slug, Snail, β-Catenin and E-cadherin), the G1/S cell cycle checkpoint (9870 and 9932, against CDK2, p-CDK2, CDK4, CDK6, Cyclin-E2, Cyclin-D1, Cdc25A and P21), the MAPK/ERK1/2 pathway (9910, 9911, 9916 and 9926, against p53, p-p53, c-Raf, p-c-Raf, MEK1/2, p-MEK1/2, ERK1/2 and p-ERK1/2), the phospho-Jak Family (97999T, against p-JAK), p-Akt (Thr308) and the NF-kB pathway (9936, against Ikkα, Ikkβ, p-Ikkα/β, p65, p-p65, IkB and p-IkB) were purchased from Cell Signaling Technology (Massachusetts, USA). *Lens culinaris agglutinin*, a lectin that can specifically identify fucose, was purchased from Vector Labs (California, USA). NSC 228155, an activator of EGFR which binds to the extracellular region of EGFR and enhance tyrosine phosphorylation of EGFR[48], was purchased from MedChemExpress (New Jersey, USA). Other chemicals and reagents were purchased from Sigma (St. Louis, USA) and Vetec (St. Louis, USA).

2.9 Plasmids and lentivirus

Four mCherry labeled shRNA fragments targeting the FUT8 gene, one GFP labeled expression clone fragment encoding the full length of the FUT8 ORF sequence and the corresponding negative control fragments were purchased from GeneCopoeia. The sequence of the shRNAs was: sh1 5′-GCCGAGAACTGTCCAAGATTC-3′, sh2 5′-GCGGAGAATAACATATCTTCA-3′, sh3 5′-GGTGTGTAATATCAACAAAGG-3′, sh4 5′-GCTTCAAACATCCAGTTATTG-3′. Lentiviral particles were generated by following a standardized protocol using highly purified plasmids and EndoFectin-Lenti™ and TiterBoost™ reagents. Viral packaging was conducted based on the recommended protocols and previous reports. The lentiviral expression construct was validated by full-length sequencing, restriction enzyme digestion and PCR-size validation using gene-specific and vector-specific primers. Four shRNA fragments targeting the EGFR gene were obtained from the Human GIPZ shRNA Bank. The sequence of the shRNAs was: Sh1 5′- AGGAACTGGATATTCTGAA-3′, sh2 5′- AGATCAGAAGACTACAAAA-3′, sh3 5′-TGGTGTGTGCAGATCGCAA-3′, sh4 5′- ACGAATATTAAACACTTCA-3′. The making of stable shEGFR expressing cell lines was conducted according to our previous reports[49, 50].

2.10 RNA extraction and RT-PCR.

Total RNA was extracted from CAFs and their paired normal lung fibroblasts (NLFs) using the TRIzol method according to previous reports[51]. A TransScript One-step gDNA Removal and cDNA Synthesis Supermix purchased from Transgene (Beijing, China) was used to synthesize first-strand cDNA. Taq Master Mix (Vazyme , Nanjing, China) was used for quantitative PCR according to the manufacturer's instructions. The reaction program was set according to the Tm values of the primers. Primer sequences were as follows: vimentin-F 5′-TGCCGTTGAAGCTGCTAACTA-3′, vimentin-R 5′-CCAGAGGGAGTGAATCCAGATTA-3′, FAP-F 5′-ATGAGCTTCCTCGTCCAATTCA-3′, FAP-R 5′-AGACCACCAGAGAGCATATTTTG-3′, α-SMA-F 5′-ATTGCCGACCGAATGCAGA-3′, α-SMA-R 5′-ATGGAGCCACCG ATCCAGAC-3′.

2.11 Western blot analysis and lectin blot analysis

Total protein was collected according to the methods described in our previous report[38]. The protein concentration of the cell lysis solution was assessed using a Thermo Fisher BCA kit. Then, 20~30 μg of total protein was run in 10% SDS-PAGE and transferred to a PVDF membrane. The samples were incubated with primary antibodies diluted to the recommended concentration overnight at 4°C. The samples were incubated with an HRP-conjugated secondary antibody at room temperature for 2 h and protein bands were detected with a chemiluminescence device. The lectin blot protocol was similar to that of the western blot, except biotinylated *Lens culinaris agglutinin* was used instead of primary antibodies.

2.12 Colony formation assay

Briefly, A549 cells or H322 cells were seeded into six-well plates (2×10^3 per well) and incubated in complete DMEM for 24 h. Then, the medium was replaced by CM with 10% FBS, and the cells were

cultured in a 37°C incubator with 5% CO_2 for 2 weeks until they grew into macroscopic colonies. Finally, the medium was removed, and the cell colonies were stained with 0.1% crystal violet and counted.

2.13 Transwell assay

After 5 continuous passages of coculture, cell migration and invasion assays were performed separately in Transwell chambers with an 8.0 μm pore size (Corning, NY, USA). The cells were starved in FBS-free DMEM overnight before they were collected and resuspended. A total of 1×10^5 A549 or H322 cells were resuspended in 250 μL of DMEM with 10% FBS and injected into the upper chamber. A total of 3×10^5 CAFs (or other fibroblasts) were resuspended in 500 μL of DMEM with 10% FBS and injected into the lower chambers. In the invasion assay, 70 uL/well of Matrigel (Corning, NY, US) diluted with DMED at a 1:5 ratio was added to the chambers prior to the experiment. After 24 h, the upper chambers were washed with PBS and dried at RT. The migrated or invaded cells on the back side of the Transwell membrane were stained with 0.1% crystal violet and the numbers of cells were recorded using a microscope.

2.14 Wound-healing assay

After 5 continuous passages of coculture, a wound-healing assay was used to test cell migration ability. NSCLC cells and fibroblasts were grown to 80%-90% confluence in the coculture plates and incubated overnight in FBS free DMEM. NSCLC cell monolayers were wounded with a sterile 100 μL pipette tip and washed with FBS free DMEM to remove detached cells from the plates. After 48 h, the medium was replaced with PBS. The wound gap was observed and photographed using a microscope, and the distance of the wound gap was measured.

2.15 Cell cycle analysis

After 5 continuous passages of coculture, cells were trypsinized and washed with PBS, resuspended in chilled methanol, and kept overnight at -20°C. Each cell sample was then resuspended in 500 μL of buffer containing 480 μL of PBS, 5 μL of RNase, 5 μL of PI and 10 μL of Triton X-100 and incubated at 37℃ for 30 minutes. After centrifugation, the cells were resuspended in PBS and filtered. Cell cycle analysis was performed using a FACS Caliber Flow Cytometer (BD Biosciences, California, US).

2.16 Immunofluorescence staining

For immunofluorescence staining, cells grown on chamber slides were washed with PBS and fixed with 4% paraformaldehyde for 15 minutes at room temperature. The samples were pretreated with Triton X-100 and incubated with 10% BSA in PBS for 30 minutes. The primary antibody against FUT8 was added to the samples, followed by incubation overnight at 4°C. Fluorescein isothiocyanate-and rhodamine-conjugated secondary antibodies and red luminous LCA were added and followed by incubation of 1 h at room temperature. DIPI was added to stain the nuclei. The samples were examined with a fluorescence microscope.

2.17 Immunoprecipitation (IP) assay

Lysates of fibroblasts were mixed with EGFR or IgG antibodies and placed on a 4℃ table shaker for overnight. Then, 40 ug protein A/G magnetic nanospheres (Santa Cruz, Texas, USA) were added in the mixture and were shaken at 4℃ for 4 h. EGFR proteins were extracted following the recommended protocols and analyzed by lectin blotting described above.

2.18 In vitro coculture assay

To obtain an appropriate initial ratio at which combined CAFs/NSCLC cells could grow continuously and maintain a proper constitution that best simulates the TME in direct contact coculture, an in vitro coculture assay was conducted. GTP (green)-labeled CAFs and mCherry (red)-labeled A549 cells were combined in test tubes and seeded in 10 cm dishes for direct contact coculture. After continuous culture for 5 passages, the cells were observed under a fluorescence microscope. The stable cell ratios were calculated as a reference to select the initial cell ratio for in vivo coinjection.

2.19 Subcutaneous co-injection tumorigenesis in nude mice

21 Female BALB/c nu+/nu+ nude mice aged 4 to 6 weeks were purchased and housed in the *Specific Pathogen Free Animal Center of Dalian Medical University*, and were divided randomly into three groups with 7 mice in each group. All procedures involving mice were approved by the *Committee for the Care and Use of Laboratory Animals of Dalian Medical University*. In this model system, fibroblasts (CAFs-NC, CAFs-shFUT8 or HLF) were mixed with epithelial cells (A549). CAFs and A549 cells were mixed at a 2:1 ratio, cast in Matrigel (total cell number of 5×10^5 in 100 uL gel) and then were injected subcutaneously into the left flank of each mouse. The tumor sizes and the weights of the mice were examined every 7 days after injection. The recombinant tissue was retrieved after a designated period of time (28 days) and analyzed. The wet weight of each recombinant tissue was recorded at harvest. The tissues were formalin-fixed, paraffin-embedded, and analyzed histologically.

2.20 Bioinformatics and gene enrichment analysis

The data used in the analysis came from the GSE22862 gene chip from the NCBI Gene Expression Omnibus (GEO)and were obtained from CAFs from the tumor tissues of 15 primary NSCLC cases. The differential expression of genes was calculated using the R pack limma. Enrichment analysis was conducted for the genes that were significantly coexpressed with the FUT8 gene ($P<0.05$) the using R package Cluster-Profiler.

2.21 Statistical analysis

Statistical data were analyzed using IBM Statistical Product and Service Solutions 25.0. The differences in clinical characteristics associated with different FUT8 expression levels were evaluated using the Chi-square Test and the Fisher Exact Probability Test. To adjust the heterogeneity of the follow-up period, survival curves were plotted on the basis of Kaplan-Meier Survival Analysis[52], and the differences between the curves were analyzed by the Log-Rank Test[53]. The Cox's Proportional Hazards Model was

applied to analyze the significance and independence of the influence of all the studied clinical and pathological factors on both tumor recurrence and cancer death risk during the follow-up period[54]. As dummy variables were established to analyze polytomous variables, the method whereby variables entered the Cox's equation was limited to the 'Enter' method, which means that all the variables entered the equation at the same time. The difference was considered to be significant at $P<0.05$.

3. Results

3.1 FUT8 was overexpressed in the CAFs of most lung adenocarcinoma cases

Totally 450 datasets were searched in the Oncomine database and 89 of them reported FUT8 expression changes in cancer vs. normal tissue. 73 out of the 89 (82%) datasets suggested that FUT8 was overexpressed in cancers, including lung, breast, colorectal, esophageal cancer. (Figure 1A).7 datasets reported FUT8 expression in lung cancer vs. normal lung. All of these datasets suggested that FUT8 was overexpressed in lung cancer. The comparison of FUT8 across the 7 analyses was shown in Supplementary figure 1A. Box charges for FUT8 expression in the 7 datasets were shown in Figure 1B~1H. Totally 963 samples were analyzed in the 7 datasets, showing that FUT8 was significantly overexpressed in adenocarcinoma rather than in any other types of lung cancer or normal lung tissues. The 7 datasets showed that FUT8 was expressed at 1.626~2.569 folds higher in lung adenocarcinomas than that in normal lung tissues.

To confirm these findings, FUT8 was tested by western blotting in 5 lung adenocarcinoma tissues and paired normal lung tissues. FUT8 was overexpressed in the tumors compared with the normal tissues in all 5 cases (Figure 1I). In the IHC staining analysis of the 135 NSCLC cases, 20 cases involving solid predominant, mucinous and micropapillary predominant lung adenocarcinomas were excluded because of failure to separate the tumor stroma from the cancerous epithelium (representative images are shown in Figure 1J). FUT8 expression was successfully evaluated in 115 cases, and representative images are shown in Figure 1L. It was found that FUT8 was overexpressed in tumor cells in almost every case, and in tumor stroma of 62 out of the 115 cases.

3.2 FUT8 expression in CAFs correlates with long-term prognosis

The baseline information and characteristics of the 115 patients are shown in Table 1. The relationship between FUT8 expression and clinicopathological factors is shown in Table 2. We found that the ratio of FUT8 positivity increased with the T staging of the tumor. The findings are not statistically significant because of limitation by the current sample size. However, statistically significant results will likely to appear when the cumulative sample size increases in future studies. The survival curves (Figure 2) indicated that, in addition to the T ($p<0.001$) and N ($p<0.000$) stages, FUT8 expression levels in CAFs can affect overall survival ($p=0.026$) and disease-free survival ($p=0.027$). These results were in accord with the univariate analysis of Cox's proportional hazard model (Table 3). Furthermore, Cox's multivariate

analysis showed that the T stage, N stage and FUT8 expression of CAFs can all serve as independent risk predicting factors for both overall and disease-free survival (Table 4).

3.3 FUT8 is overexpressed in CAFs and mediates high levels of CF

Five pairs of CAFs/NLFs were successfully isolated. Representative morphological characteristics observe in the comparison of primary CAFs with primary NLFs and lab-grown HLF cells are shown in Supplementary figure 1B. Primary fibroblasts were longer and thinner. Although some previous reports have indicated that morphological differences exist between CAFs and NLFs[55-57], no significant differences were observed in the current study. The isolated primary fibroblasts were identified on the basis of specific markers of myofibroblasts (Figure 3A), showing that phenotypic differences existed between CAFs and NLFs. Western blotting showed that FUT8 was overexpressed in 4 out of 5 CAFs (P01, P03, P07, P08) compared with the corresponding NLFs (Figure 3B). lectin blotting (LCA) showed coincident results of increased CF in the 4 pairs of primary fibroblasts (Figure 3C). As a result, The CAFs of P03, which probably showed the most significant difference in CF between CAFs and NLFs, were selected for the following study.

FUT8 and ST6Gal1 (key enzyme for sialic acid glycosylation) were tested by western blotting in CAFs and three frequently-used lab-grown human normal lung fibroblast cell lines (MRC5, HLF1 and HLF, Figure 3D, 3E). FUT8 and ST6Gal1 together catalyze most glycosylation modifications in mammals[58]. These results indicated that the general glycosylation level in CAF is higher than that in normal lung fibroblasts. HLFs exhibited the lowest glycosylase level and the weakest myofibroblast phenotype. Thus, HLF cells were selected as the control cell line for comparison with the CAFs, as NLFs was very difficult to culture continuously in vitro. To visually observe the relationship between FUT8 and CF, immunofluorescence and lectin fluorescence staining was conducted in P03 CAFs and NLFs, and lab-grown HLF cells were used as a control (Figure 3F). FUT8 was overexpressed in both the cytoplasm and nucleus of CAFs and was expressed at low levels in NLFs and HLF cells. It was interesting that secretory vesicles containing large amounts of FUT8 were observed in CAFs (indicated by white arrows in the zoomed images). These results suggested that the posttranslational CF modification of both secretory proteins and intracellular proteins was very active in CAFs.

3.4 FUT8 in CAFs was necessary for the construction of an invasive tumor microenvironment in vivo

Four shRNA fragments were used for downregulating FUT8 in CAFs and the effects of gene intervention were tested by western blotting (Figure 4A). Sh4 was used for producing the stably shFUT8-expressing CAFs. Lectin blotting showed that CF levels were downregulated in CAFs-shFUT8 (Figure 4B).

For animal pre-experiments, an in vitro coculture assay was conducted. In previous articles, inappropriate coinjection ratios often resulted in the absence of fibroblasts or too few tumor cells in the generated tumors. Thus, it is important to investigate a proper ratio for the cell mixture. According to the results, a ratio of CAFs:A549 = 2:1, which stably mimics a TME similar to that of primary lung cancer, was selected as the initial ratio for subcutaneous coinjection into nude mice (Figure 4C). After 28 days of observation,

the tumors were removed (Figure 4F). The recorded changes in body weight and tumor diameter and the final masses of the tumors are shown in Figure D~E, G. The growth of CAF-NC tumors was significantly faster than that of tumors in the control group (HLF). However, tumor growth was dramatically blocked by the downregulation of FUT8 in CAFs.

Furthermore, IHC staining showed the interior structure of the reconstructed tumors. The sites and extents of the stroma were clearly marked by α-SMA staining. It was interesting to find that the cancerous epithelium was more mixed with the stroma in the CAF-NC/A549 tumors. In the CAF-shFUT8/A549 tumors and HLF/A549 tumors, the tumor cells preferred to clump together rather than invade the stroma (Figure 4H). This finding was most obvious at the junctions between the epithelial tissues and the stroma indicated by white and black arrows in Figure 4H. Cancer cells rarely invaded the stroma in the CAF-shFUT8/A549 tumors. The invasion of cancer cells was slightly more obvious in the HLF/A549 tumors and was most obvious in the CAFs-NC/A549 tumors.

3.5 CF mediated by FUT8 is necessary for maintaining the protumorigenic capacity of CAFs

FUT8 was upregulated in the stably FUT8-overexpressing HLFs (Figure 5A). Lectin blotting showed that CF levels were upregulated in CAF-FUT8 OE cells (Figure 4B). A549 and H322 were treated with conditioned medium of fibroblasts. The downregulation of FUT8 in CAFs dramatically reduced their ability to promote the cell proliferation of NSCLC cells, while the upregulation of FUT8 in HLFs slightly increased this ability (Figure 4C). The Transwell migration and invasion (matrigel) assays showed that the downregulation of FUT8 in CAFs dramatically reduced the migration and invasion of cocultured NSCLC cells, while the upregulation of FUT8 in HLFs only caused slightly increased migration in H322 cells (Figure 4D,4E).

Non-contact coculture system was successfully established. A concise 3D printing illustration of the prototype coculture device design is shown in Figure 4F, and the improved design of this device used in the current study is shown in Supplementary Figure 1C. Evaluation of the efficiency of solute exchange showed that the diffusion time of the standard protein solution was 40 to 50 minutes (Supplementary Figure 1D).As the change in migration abilities was significant, the results regarding cell migration were reconfirmed in the wound healing assays using the non-contact coculture system (Figure 4G).

The AO/EB assay showed that the downregulation of FUT8 in CAFs and upregulation of FUT8 in HLFs didn’t resulted in change of number of apoptotic H322 cells in the non-contact coculture system (Supplementary figure 2A). This result was confirmed by AV/PI staining and flow cytometry apoptosis assays (Supplementary figure 2B).

PI Staining and flow cytometry analysis showed that the downregulation of FUT8 in CAFs led to blockage of the G1/S checkpoint in NSCLC cells in the non-contact coculture system, as the ratio of cells in G0/G1 increased, while the ratio of cells in S phase decreased. However, no change in the regulation of cell cycle of NSCLC cells could be observed when FUT8 was upregulated in the cocultured HLFs (Figure 5H). The results implied that G2/M blockage had probably occurred as diploids were observed in H322 cells and

part of A549 cells (yellow peaks); however, this was not supported by enough molecular evidence (data not shown). The results implied that FUT8/CF was necessary but insufficient for lung fibroblasts to acquire the capacity to promote the cell cycle of NSCLC cells.

To explain these findings, signaling pathways of NF-kB, MAPK/ERK1/2, Biomarkers of EMT and cell cycle G1/S checkpoint in A549 cells in the non-contact coculture system were tested by western blotting. (Figure 5I~L). The results showed that the downregulation of FUT8 in CAFs led to dramatic inhibition of these signalings in NSCLC cells in the non-contact coculture system, while HLF-FUT8 OE cells didn't show a matching increase in these signalings. This result is in accord with the change in proliferation, migration, invasion, and cell cycle of NSCLC cells in the non-contact coculture system, and supports the fact that high-FUT8/CF CAFs help to construct a more invasive TME. However, this finding also suggested that only upregulation of CF modification in HLFs cannot make them to become as protumorigenic as CAFs.

3.6 Potential mechanisms of FUT8 maintaining the tumor-promoting phenotype of CAFs

Although it is believed that CAFs most likely promote the growth of tumors in a paracrine manner, we noted that it was also important that CAFs maintained their cancer-promoting phenotype in dynamic symbiosis with tumor cells. To explain the potential mechanisms by which FUT8 acts to maintain the tumor-promoting phenotype of CAFs, we analyzed the gene microarray data from the GEO which contains the genome data of 15 CAF cell lines. Kyoto Encyclopedia of Genes and Genomes (KEGG) analysis predicted 20 biochemical functional domains that were significantly regulated by FUT8/CF activity in CAFs (Supplementary Figure 6A). Gene set enrichment analysis (GSEA) was carried out, showing that 4 signaling pathways were regulated by the FUT8/CF activity in CAFs (Figure 6A, B, C, D). Among the 4 pathways, the ErbB tyrosine kinase receptor family pathway, the apoptosis regulation network and the β-alanine metabolism pathway were upregulated, while the neuroactive ligand-receptors pathway was downregulated by the overexpression of FUT8/CF. The heatmap showed an intuitive view of the activation of the ErbB pathway by FUT8/CF (Figure 6E), and the heatmaps of the other three altered pathways are shown in the supplementary data. The further analysis showed that the increase of gene copies occurred in none of the ErbB genes (EGFR, HER2, HER3 and HER4). However, the gene copies of downstream signal factors such as PIK3CA (PI3Kp110α), PIK3CB (PI3Kp110β), PTEN, MTOR (mTOR), STAT3, STAT5A and STAT5B were increased significantly in FUT8 high-expressing CAFs (Figure 6F).

3.7 CF mediated by FUT8 regulates cancer-promoting capacities of CAFs via the modification of EGFR fucosylation

As EGFR and its downstream signaling molecules are mostly activated by phosphorylation modifications, it was essential to reconfirm the regulation of FUT8/CF modification on EGFR and its downstream signalings. EGFR, p-EGFR and FUT8 in the 5 pairs of primary CAFs/NLFs were tested by western blotting (Figure 7A). The expression of EGFR showed no change between CAFs and NLFs, while p-EGFR was consistent with the expression of FUT8. Four shRNA fragments were used for downregulating FUT8 in CAFs and the effects of gene intervention were tested by western blotting (Figure 7B). Sh2 was used for

producing the stably shEGFR CAFs. The binding of fucose to EGFR was tested by immunoprecipitation and lectin blotting (Figure 7C). EGFR was successfully enriched and the fucose binding to EGFR was consistent with the expression of FUT8, which reconfirmed the fucoglycosylated modification of EGFR. Rescue experiments were conducted respectively in CAFs and HLFs, and the results are shown in Figure 7D, E, which strongly support that EGFR and its downstream signalings are regulated by FUT8/CF modification. Further, clone formation assay showed that downregulation of EGFR tyrosine phosphorylation led to reduced cancer-promoting capacity of CAFs(Figure 7F), and counteraction of the cancer-promoting capacity of FUT8 overexpressing HLFs (Figure 7G).

4. Discussion

As the most abundant component of the TME, CAFs are considered to be responsible for the tumor promoting effects of the TME. CAFs influence NSCLC cells by secreting a variety of cytokines, thereby affecting the proliferation, migration, invasion and other biological behaviors of NSCLC cells. In addition, cancer cells participate in positive feedback with the activation and maintenance of the cancer-associated properties of CAFs[59]. In the current study, we aimed to investigate the effect of FUT8/CF on the maintenance of the cancer-associated properties of CAFs, and their potential use in the determination of prognosis and molecular therapy. Researchers have tried many methods for stimulating the tumor microenvironment both in vivo and in vitro, especially for restoring the interaction between CAFs and tumor cells. Classic models include the use of conditioned medium, the Transwell system[60], the Boyden chamber system[61], and xenoanimal coinjection models[62]. In recent years, microfluidic chip technology[63] and the patient-derived xenograft mouse model [64] (PDX) have also become common research tools. In the current study, we introduced a novel noncontact coculture device, that overcomes the limitations of previous models in terms of cell quantities and passages, and its practicality was experimentally verified.

Consistent with previous reports, the current study showed that FUT8 was overexpressed in NSCLC tissues. Moreover, FUT8 was overexpressed not only in cancerous epithelial cells (NSCLC cells) but also in the tumor stroma (CAFs) in more than half of the NSCLC cases. Although the FUT8 overexpression in CAFs was not as high as that in NSCLC cells in these cases, it was clearly higher than in the paired normal lung tissues. Based on our finding in previous studies that CF mediated by FUT8 plays a key role in the transformation of pericytes and fibroblasts into myofibroblasts, we assumed that FUT8 functions similarly in the activation and maintenance of CAFs. More importantly, we confirmed FUT8 expression in CAFs as an independent risk factor for long-term prognosis in 115 patients who were retrospectively observed. These results implied that patients with high FUT8 in CAFs likely had tumors that were so aggressive and metastatic that they had already formed micrometastases that could not be detected by screening before surgical treatments.

To investigate the effects of FUT8 on CAFs, we extracted primary CAFs and NLFs from very aggressive NSCLC with a clinical stage of at least IIIA. For example, the CAFs used in the functional and mechanism experiments (P03) were extracted from a female patient with stage IIIA lung adenocarcinoma. It was

found that FUT8 and CF were upregulated in more than half of those CAFs compared with their paired NLFs. In addition, the level of CF was largely consistent with the expression of FUT8 in these primary cell lines. It was interesting that secretory vesicles containing abundant FUT8 were observed in CAFs rather than in NLFs or lab-grown HLFs. This implied that the fucosylation of secretory proteins was much more active in CAFs compared with NLFs and HLF.

In the current study, the silencing of FUT8 in CAFs and the upregulation of FUT8 in HLFs affected the biofunctions of the cocultured NSCLC cells. This paper is the first to provide images of the histological structure of an artificial TME in mice subjected to subcutaneous coinjection of CAFs/NSCLC. The cell mixture of CAFs-NC/A549 cells showed dramatic tumor formation and growth abilities compared with the CAF-shFUT8/A549 and HLF/A549 (control group) cells. To our surprise, IHC staining showed a very invasive microenvironment inside the tumors generated by CAFs-NC /A549 cells. In contrast, the of CAF-shFU8/A549 tumors exhibited a very inactive microenvironment in which the NSCLC cells showed almost no invasion into the stroma and compacted into clumps.

Later we noted the effect on tumor proliferation regulated by FUT8 in CAFs in vitro. It was assumed that there are two possible reasons for this effect: FUT8 in CAFs inhibits the apoptosis of NSCLC, or FUT8 in CAFs positively regulates the cell cycle of NSCLC. Unfortunately, the apoptosis assays led to rejection of the first hypothesis. On the other hand, the cell cycle assays indicated that the downregulation of FUT8 in CAFs induced cell cycle blockage in NSCLC. Analysis showed that this block occurred at the G1/S checkpoint, during which the cells complete their preparation of DNA synthesis and enter S phase to begin synthesis. The assessment of G1/S biomarkers confirmed this finding. This result implied that G2/M blockage had probably occurred, as diploids were observed in NSCLC cells. However, this possibility was not supported by enough molecular evidence. The effects on tumor migration and invasion were first demonstrated by wound healing assays and Tranwell assays. It was also molecularly proved that FUT8 in CAFs/HLFs had a positive effect on NSCLC in regard to EMT. The presence of FUT8 in fibroblasts leads to the high level of CF and subsequently increasing the capacity of CAFs to induce the EMT of NSCLC cells, thereby enhancing tumor migration and invasion. In addition, significant change in the either cell cycle or migration/invasion was rarely observed in NSCLC cells cocultures with HLF-NC/HLF-FUT8 OE, implying that although FUT8 was essential for CAFs to affect the cell cycle of NSCLC cells, upregulation of FUT8 alone without systematic activation does not confer the same capacity upon HLFs.

The above results are supported by the test of signalings of NF-kB, MAPK/ERK1/2, EMT and cell cycle G1/S checkpoint in A549 cells cocultured with fibroblasts in the non-contact coculture system. The 4 signalings are respectively responsible for cell proliferation, formation of an inflammatory environment, cell migration and regulation of cell cycle. The downregulation of FUT8/CF in CAFs led to significant inhibition considerably upstream of the 4 signalings, which probably contributed to the blockage of the cell cycle, inhibition of EMT, and the less invasive microenvironment, thereby causing slowed growth and delayed progression of NSCLC. However, molecular change in NSCLC cells cocultures with HLF-NC/HLF-

FUT8 OE was also less significant compared with that of NSCLC cells cocultures with CAF-NC/CAFF-shFUT8.

It was showed by the GSEA that the low expression of FUT8/CF led to inhibition of both extrinsic and intrinsic apoptosis pathways. There has been a debate about the effect of FUT8/CF on cell apoptosis in different types of cell and tissue as some researchers reported promotion[66-68], and one reported inhibition[69]. However, whether it was the reason of the inhibited capacity of FUT8 low-expressing CAFs remains unknown. Moreover, the inhibition of the ErbB pathway may be more important for the inhibited cancer-promoting capacities of FUT8 low-expressing CAFs, as it blocked multiple growth factor signals[70] that were previously proved to be necessary for the activation and maintenance of CAFs, including EGF, TGF-α, NRG1 and so on. The unchanged gene copy numbers of the ErbB genes implied that the activity of these genes was not regulated at the level of transcription and translation. As was reported in previous articles that the EGFR can only function if it is properly glycosylated[28, 71], it is considered that the downregulation of FUT8 blocked core fucosylation of the ErbBs and as a result inhibited the signals to activate the downstream pathways such as the PI3K/AKT/mTOR, JAK/STAT and MAPK/ERK1/2. Additionally, although the downregulated β-alanine metabolism pathway and the upregulated neuroactive ligand-receptors (with down-regulated FUT8/CF) are not closely related to tumor progression, we noted that a lot of genes responsible for cell metabolism and biosynthesis were altered. However, the significance and mechanisms of these findings remained to be investigated.

Finally, the hypothesis based on the result of GSEA that EGFR was regulated by FUT8/CF in CAFs has been verified by in vitro experiments. In addition to the constant expression level of EGFR in different primary lung fibroblasts, the consistency of EGFR phosphorylation and FUT8 expression level indicated that the gene was likely modified by CF. This mechanism was confirmed by further immunoprecipitation and lection blotting. Most importantly, the relationship between EGFR activation and the phosphorylation of its downstream major signal transducers, including ERK, JAK and Akt, were tested in the rescue experiments by western blotting and in vitro coculture proliferation assays.

Conclusion

The current study has provided a complete collection of evidence to prove that CF mediated by FUT8 in CAFs is essential for CAFs to acquire and maintain the ability to promote the development and progression of NSCLC. FUT8 is overexpressed in the TME in the majority of cases of lung adenocarcinomas, and is an independent risk factor for long-term prognosis. FUT8/CF in CAFs is responsible for the cancer-promoting capacities of CAFs and lead to a malignant tumor microenvironment, in which NSCLC cells show faster cell proliferation and greater aggressiveness. CF modification enhances tyrosine phosphorylation of EGFR in CAFs, which causes activation of downstream signalings of EGFR and maintains cancer-promoting properties of CAFs.

List Of Abbreviations

NSCLC: non-small cell lung cancer

CAFs: cancer-associated fibroblasts

TME: tumor microenvironment

FUT8: fucosyltransferase 8, α1,6-fucosyltransferase

CF: core α1,6-fucosylation

GEO: Gene Expression Omnibus

EMT: epithelial-mesenchymal transition

MAPK/ERK: Mitogen-activated protein kinase/ extracellular signal-regulated kinase

NF-kB: nuclear factor kappa-B

α-SMA: alpha smooth muscle actin

FAP: fibroblast activating protein

GDP: guanosine diphosphate

GlcNAc: N- acetylglucosamine

DAB: 3,3'-diaminobenzidine

DMEM: Dulbecco's modified Eagle medium

Declarations

Ethics approval and consent to participate

The study was approved by the Medical Ethical Committees of the First Hospital of Dalian Medical University and the Committee for the Care and Use of Laboratory Animals of Dalian Medical University.

Consent for publication

Not applicable

Data availability statements

The datasets used and/or analysed during the current study are available from the corresponding author on reasonable request.

Competing interests

No conflict of interest exits in the submission of this manuscript, and manuscript is approved by all authors for publication.The work described in this paper was original research that has not been published previously, and not under consideration for publication elsewhere, in whole or in part.

Funding

This work was supported by grants from the National Natural Science Foundation of China (81670063) .

Authors' contributions

Fengzhou Li, Zhuoshi Li and Zhe Sun analyzed and interpreted the patient data. Wei Guo, Wendan Yu, and Jiaqi Qiang are professional pathologists responsible for the pathological diagnosis of the immunohistochemical staining assays. Fengzhou Li, Shilei Zhao, Yanwei Cui and Wei Sun conducted most of the laboratory experiments. Lei Fang, Zhuoshi Li and Qiang Xie conducted all the in vivo experiments. Prof. Wuguo Deng, Prof. Chundong Gu and Prof. Taihua Wu are the supervisors of the project and they also contributed in writing and revising the paper. All authors read and approved the final manuscript.

Acknowledgements

We would like to acknowledge my colleagues from Dalian Medical University and Prof. Xiaohui Zhang from Dalian University for their great help to our research. We especially like to acknowledge all the researchers from Deng lab of the Institute of Cancer Stem Cells of Dalian Medical University for their excellent technical assistance. This work was supported by grants from the National Natural Science Foundation of China (81670063) .

References

[1] Siegel RL, Miller KD, Jemal A. Cancer statistics, 2018. CA Cancer J Clin. 2018. 68(1): 7-30.

[2] Li F, Zhang S, Zhang Q, Li J, Zhao S, Gu C. CYP1B1 G199T Polymorphism Affects Prognosis of NSCLC Patients with the Potential to Be an Indicator and Target for Precise Drug Intervention. Biomed Res Int. 2017. 2017: 1529564.

[3] Yu T, Guo Z, Fan H, Song J, Liu Y, Gao Z, Wang Q. Cancer-associated fibroblasts promote non-small cell lung cancer cell invasion by upregulation of glucose-regulated protein 78 (GRP78) expression in an integrated bionic microfluidic device. Oncotarget. 2016. 7(18): 25593-603.

[4] Ben Amar J, Ben Safta B, Zaibi H, Dhahri B, Baccar MA, Azzabi S. Prognostic factors of advanced stage non-small-cell lung cancer. Tunis Med. 2016. 94(5): 360-367.

[5] Huang Y, Lin D, Taniguchi CM. Hypoxia inducible factor (HIF) in the tumor microenvironment: friend or foe. Sci China Life Sci. 2017. 60(10): 1114-1124.

[6] Berdiel-Acer M, Sanz-Pamplona R, Calon A, Cuadras D, Berenguer A, Sanjuan X, Paules MJ, Salazar R, Moreno V, Batlle E, Villanueva A, Molleví DG. Differences between CAFs and their paired NCF from adjacent colonic mucosa reveal functional heterogeneity of CAFs, providing prognostic information. Mol Oncol. 2014. 8(7): 1290-305.

[7] Vicent S, Sayles LC, Vaka D, Khatri P, Gevaert O, Chen R, Zheng Y, Gillespie AK, Clarke N, Xu Y, Shrager J, Hoang CD, Plevritis S, Butte AJ, Sweet-Cordero EA. Cross-species functional analysis of cancer-associated fibroblasts identifies a critical role for CLCF1 and IL-6 in non-small cell lung cancer in vivo. Cancer Res. 2012. 72(22): 5744-56.

[8] Goicoechea SM, García-Mata R, Staub J, et al. Palladin promotes invasion of pancreatic cancer cells by enhancing invadopodia formation in cancer-associated fibroblasts. Oncogene. 2014. 33(10): 1265-73.

[9] Liao Z, Tan ZW, Zhu P, Tan NS. Cancer-associated fibroblasts in tumor microenvironment - Accomplices in tumor malignancy. Cell Immunol. 2018 .

[10] Son B, Lee S, Youn H, Kim E, Kim W, Youn B. The role of tumor microenvironment in therapeutic resistance. Oncotarget. 2017. 8(3): 3933-3945.

[11] Wang Y, Fukuda T, Isaji T, Lu J, Im S, Hang Q, Gu W, Hou S, Ohtsubo K, Gu J. Loss of α,1,6-fucosyltransferaseinhibits chemical-induced hepatocellular carcinoma and tumorigenesis by down-regulating several cell signaling pathways. FASEB J. 2015. 29(8): 3217-27.

[12] Bernardi C, Soffientini U, Piacente F, Tonetti MG. Effects of microRNAs on fucosyltransferase 8 (FUT8) expression in hepatocarcinoma cells. PLoS One. 2013. 8(10): e76540.

[13] Cheng L, Luo S, Jin C, Ma H, Zhou H, Jia L. FUT family mediates the multidrug resistance of human hepatocellular carcinoma via the PI3K/Akt signaling pathway. Cell Death Dis. 2013. 4: e923.

[14] Tu CF, Wu MY, Lin YC, Kannagi R, Yang RB. FUT8 promotes breast cancer cell invasiveness by remodeling TGF-β receptor core fucosylation. Breast Cancer Res. 2017. 19(1): 111.

[15] Yang Q, Wang LX. Mammalian α-1,6-Fucosyltransferase (FUT8) Is the Sole Enzyme Responsible for the N-Acetylglucosaminyltransferase I-independent Core Fucosylation of High-mannose N-Glycans. J Biol Chem. 2016. 291(21): 11064-71.

[16] Honma R, Kinoshita I, Miyoshi E, Tomaru U, Matsuno Y, Shimizu Y, Takeuchi S, Kobayashi Y, Kaga K, Taniguchi N, Dosaka-Akita H. Expression of fucosyltransferase 8 is associated with an unfavorable clinical outcome in non-small cell lung cancers. Oncology. 2015. 88(5): 298-308.

[17] Yue L, Han C, Li Z, Li X, Liu D, Liu S, Yu H. Fucosyltransferase 8 expression in breast cancer patients: A high throughput tissue microarray analysis. Histol Histopathol. 2016. 31(5): 547-55.

[18] Hu P, Shi B, Geng F, Zhang C, Wu W, Wu XZ. E-cadherin core fucosylation regulates nuclear beta-catenin accumulation in lung cancer cells. Glycoconj J. 2008. 25(9): 843-50.

[19] Kossowska B, Ferens-Sieczkowska M, Gancarz R, Passowicz-Muszyńska E, Jankowska R. Fucosylation of serum glycoproteins in lung cancer patients. Clin Chem Lab Med. 2005. 43(4): 361-9.

[20] Liu YC, Yen HY, Chen CY, Chen CH, Cheng PF, Juan YH, Chen CH, Khoo KH, Yu CJ, Yang PC, Hsu TL, Wong CH. Sialylation and fucosylation of epidermal growth factor receptor suppress its dimerization and activation in lung cancer cells. Proc Natl Acad Sci U S A. 2011. 108(28): 11332-7.

[21] Gandhi J, Zhang J, Xie Y, Soh J, Shigematsu H, Zhang W, Yamamoto H, Peyton M, Girard L, Lockwood WW, Lam WL, Varella-Garcia M, Minna JD, Gazdar AF. Alterations in genes of the EGFR signaling pathway and their relationship to EGFR tyrosine kinase inhibitor sensitivity in lung cancer cell lines. PLoS One. 2009. 4(2): e4576.

[22] Andersson U, Schwartzbaum J, Wiklund F, Sjöström S, Liu Y, Tsavachidis S, Ahlbom A, Auvinen A, Collatz-Laier H, Feychting M, Johansen C, Kiuru A, Lönn S, Schoemaker MJ, Swerdlow AJ, Henriksson R, Bondy M, Melin B. A comprehensive study of the association between the EGFR and ERBB2 genes and glioma risk. Acta Oncol. 2010. 49(6): 767-75.

[23] Pisano A, Santolla MF, De Francesco EM, De Marco P, Rigiracciolo DC, Perri MG, Vivacqua A, Abonante S, Cappello AR, Dolce V, Belfiore A, Maggiolini M, Lappano R. GPER, IGF-IR, and EGFR transduction signaling are involved in stimulatory effects of zinc in breast cancer cells and cancer-associated fibroblasts. Mol Carcinog. 2017. 56(2): 580-593.

[24] Luo H, Yang G, Yu T, Luo S, Wu C, Sun Y, Liu M, Tu G. GPER-mediated proliferation and estradiol production in breast cancer-associated fibroblasts. Endocr Relat Cancer. 2014. 21(2): 355-69.

[25] Álvarez-Teijeiro S, García-Inclán C, Villaronga MÁ, Casado P, Hermida-Prado F, Granda-Díaz R, Rodrigo JP, Calvo F, Del-Río-Ibisate N, Gandarillas A, Morís F, Hermsen M, Cutillas P, García-Pedrero JM. Factors Secreted by Cancer-Associated Fibroblasts that Sustain Cancer Stem Properties in Head and Neck Squamous Carcinoma Cells as Potential Therapeutic Targets. Cancers (Basel). 2018. 10(9).

[26] Norman J, Badie-Dezfooly B, Nord EP, Kurtz I, Schlosser J, Chaudhari A, Fine LG. EGF-induced mitogenesis in proximal tubular cells: potentiation by angiotensin II. Am J Physiol. 1987. 253(2 Pt 2): F299-309.

[27] Matsumoto K, Yokote H, Arao T, Maegawa M, Tanaka K, Fujita Y, Shimizu C, Hanafusa T, Fujiwara Y, Nishio K. N-Glycan fucosylation of epidermal growth factor receptor modulates receptor activity and sensitivity to epidermal growth factor receptor tyrosine kinase inhibitor. Cancer Sci. 2008. 99(8): 1611-7.

[28] Wang X, Gu J, Ihara H, Miyoshi E, Honke K, Taniguchi N. Core fucosylation regulates epidermal growth factor receptor-mediated intracellular signaling. J Biol Chem. 2006. 281(5): 2572-7.

[29] Suzuki E, Yamazaki S, Naito T, Hashimoto H, Okubo S, Udagawa H, Goto K, Tsuboi M, Ochiai A, Ishii G. Secretion of high amounts of hepatocyte growth factor is a characteristic feature of cancer-associated fibroblasts with EGFR-TKI resistance-promoting phenotype-A study of 18 cases of cancer-associated fibroblasts. Pathol Int. 2019 .

[30] Yi Y, Zeng S, Wang Z, Wu M, Ma Y, Ye X, Zhang B, Liu H. Cancer-associated fibroblasts promote epithelial-mesenchymal transition and EGFR-TKI resistance of non-small cell lung cancers via HGF/IGF-1/ANXA2 signaling. Biochim Biophys Acta Mol Basis Dis. 2018. 1864(3): 793-803.

[31] Gao MQ, Kim BG, Kang S, Choi YP, Yoon JH, Cho NH. Human breast cancer-associated fibroblasts enhance cancer cell proliferation through increased TGF-α cleavage by ADAM17. Cancer Lett. 2013. 336(1): 240-6.

[32] Han ME, Kim HJ, Shin DH, Hwang SH, Kang CD, Oh SO. Overexpression of NRG1 promotes progression of gastric cancer by regulating the self-renewal of cancer stem cells. J Gastroenterol. 2015. 50(6): 645-56.

[33] Sun W, Tang H, Gao L, Sun X, Liu J, Wang W, Wu T, Lin H. Mechanisms of pulmonary fibrosis induced by core fucosylation in pericytes. Int J Biochem Cell Biol. 2017. 88: 44-54.

[34] Hou GX, Liu P, Yang J, Wen S. Mining expression and prognosis of topoisomerase isoforms in non-small-cell lung cancer by using Oncomine and Kaplan-Meier plotter. PLoS One. 2017. 12(3): e0174515.

[35] Liu W, Ouyang S, Zhou Z, Wang M, Wang T, Qi Y, Zhao C, Chen K, Dai L. Identification of genes associated with cancer progression and prognosis in lung adenocarcinoma: Analyses based on microarray from Oncomine and The Cancer Genome Atlas databases. Mol Genet Genomic Med. 2019. 7(2): e00528.

[36] Xu B, Liu N, Chen SQ, Jiang H, Zhang LJ, Zhang XW, Yang Y, Sha GZ, Liu J, Zhu WD, Chen M. Expression of SRD5A1 and its prognostic role in prostate cancer: Analysis based on the data-mining of ONCOMINE. Zhonghua Nan Ke Xue. 2016. 22(9): 771-776.

[37] Asamura H, Chansky K, Crowley J, Goldstraw P, Rusch VW, Vansteenkiste JF, Watanabe H, Wu YL, Zielinski M, Ball D, Rami-Porta R. The International Association for the Study of Lung Cancer Lung Cancer Staging Project: Proposals for the Revision of the N Descriptors in the Forthcoming 8th Edition of the TNM Classification for Lung Cancer. J Thorac Oncol. 2015. 10(12): 1675-84.

[38] Zhao S, Guo W, Li J, Yu W, Guo T, Deng W, Gu C. High expression of Y-box-binding protein 1 correlates with poor prognosis and early recurrence in patients with small invasive lung adenocarcinoma. Onco Targets Ther. 2016. 9: 2683-92.

[39] Zhao S, Guo T, Li J, Uramoto H, Guan H, Deng W, Gu C. Expression and prognostic value of GalNAc-T3 in patients with completely resected small (≤2 cm) peripheral lung adenocarcinoma after

IASLC/ATS/ERS classification. Onco Targets Ther. 2015. 8: 3143-52.

[40] Travis WD, Brambilla E, Burke AP, Marx A, Nicholson AG. Introduction to The 2015 World Health Organization Classification of Tumors of the Lung, Pleura, Thymus, and Heart. J Thorac Oncol. 2015. 10(9): 1240-1242.

[41] Travis WD, Brambilla E, Noguchi M, Nicholson AG, Geisinger KR, Yatabe Y, Beer DG, Powell CA, Riely GJ, Van Schil PE, Garg K, Austin JH, Asamura H, Rusch VW, Hirsch FR, Scagliotti G, Mitsudomi T, Huber RM, Ishikawa Y, Jett J, Sanchez-Cespedes M, Sculier JP, Takahashi T, Tsuboi M, Vansteenkiste J, Wistuba I, Yang PC, Aberle D, Brambilla C, Flieder D, Franklin W, Gazdar A, Gould M, Hasleton P, Henderson D, Johnson B, Johnson D, Kerr K, Kuriyama K, Lee JS, Miller VA, Petersen I, Roggli V, Rosell R, Saijo N, Thunnissen E, Tsao M, Yankelewitz D. International association for the study of lung cancer/american thoracic society/european respiratory society international multidisciplinary classification of lung adenocarcinoma. J Thorac Oncol. 2011. 6(2): 244-85.

[42] Liu L, Liu L, Yao HH, Zhu ZQ, Ning ZL, Huang Q. Stromal Myofibroblasts Are Associated with Poor Prognosis in Solid Cancers: A Meta-Analysis of Published Studies. PLoS One. 2016. 11(7): e0159947.

[43] Kilvaer TK, Khanehkenari MR, Hellevik T, Al-Saad S, Paulsen EE, Bremnes RM, Busund LT, Donnem T, Martinez IZ. Cancer Associated Fibroblasts in Stage I-IIIA NSCLC: Prognostic Impact and Their Correlations with Tumor Molecular Markers. PLoS One. 2015. 10(8): e0134965.

[44] Tsujino T, Seshimo I, Yamamoto H, Ngan CY, Ezumi K, Takemasa I, Ikeda M, Sekimoto M, Matsuura N, Monden M. Stromal myofibroblasts predict disease recurrence for colorectal cancer. Clin Cancer Res. 2007. 13(7): 2082-90.

[45] Yamashita M, Ogawa T, Zhang X, Hanamura N, Kashikura Y, Takamura M, Yoneda M, Shiraishi T. Role of stromal myofibroblasts in invasive breast cancer: stromal expression of alpha-smooth muscle actin correlates with worse clinical outcome. Breast Cancer. 2012. 19(2): 170-6.

[46] Inoue C, Tamatsuki D, Miki Y, Saito R, Okada Y, Sasano H. Prognostic significance of combining immunohistochemical markers for cancer-associated fibroblasts in lung adenocarcinoma tissue. Virchows Arch. 2019. 475(2): 181-189.

[47] Li F, Zhao S, Guo T, Li J, Gu C. The Nutritional Cytokine Leptin Promotes NSCLC by Activating the PI3K/AKT and MAPK/ERK Pathways in NSCLC Cells in a Paracrine Manner. Biomed Res Int. 2019. 2019: 2585743.

[48] Sakanyan V, Hulin P, Alves de Sousa R, Silva VA, Hambardzumyan A, Nedellec S, Tomasoni C, Logé C, Pineau C, Roussakis C, Fleury F, Artaud I. Activation of EGFR by small compounds through coupling the generation of hydrogen peroxide to stable dimerization of Cu/Zn SOD1. Sci Rep. 2016. 6: 21088.

[49] Zhao S, Wang Y, Guo T, Yu W, Li J, Tang Z, Yu Z, Zhao L, Zhang Y, Wang Z, Wang P, Li Y, Li F, Sun Z, Xuan Y, Tang R, Deng WG, Guo W, Gu C. YBX1 regulates tumor growth via CDC25a pathway in human lung adenocarcinoma. Oncotarget. 2016 .

[50] Guo T, Zhao S, Wang P, Xue X, Zhang Y, Yang M, Li N, Li Z, Xu L, Jiang L, Zhao L, Ma PC, Rosell R, Li J, Gu C. YB-1 regulates tumor growth by promoting MACC1/c-Met pathway in human lung adenocarcinoma. Oncotarget. 2017 .

[51] Rio DC, Ares M, Hannon GJ, Nilsen TW. Purification of RNA using TRIzol (TRI reagent). Cold Spring Harb Protoc. 2010. 2010(6): pdb.prot5439.

[52] E. L. Kaplan PM. Nonparametric Estimation from Incomplete Observations. J Am Stat Assoc. 1958. (53): 457-481.

[53] Design and analysis of randomised clinical trials requiring prolonged observation of each patient. Br J Cancer. 1977. (35): 1-39.

[54] Cox DR. Regression models and life tables regression models and life tables. J R Stat Soc. 1972. (34): 187-220.

[55] 16.8.12 Clonal heterogeneity in osteogenic potential of lung cancer associated fibroblasts[PMIDZ27119516]. 2016 .

[56] Horie M, Saito A, Mikami Y, Ohshima M, Morishita Y, Nakajima J, Kohyama T, Nagase T. 16.8.10 Characterization of human lung cancer-associated fibroblasts in three-dimensional in vitro co-culture model. Biochem Biophys Res Commun. 2012. 423(1): 158-63.

[57] Kim SH, Choe C, Shin YS, Jeon MJ, Choi SJ, Lee J, Bae GY, Cha HJ, Kim J. Human lung cancer-associated fibroblasts enhance motility of non-small cell lung cancer cells in co-culture. Anticancer Res. 2013. 33(5): 2001-9.

[58] Hirao Y, Matsuzaki H, Iwaki J, Kuno A, Kaji H, Ohkura T, Togayachi A, Abe M, Nomura M, Noguchi M, Ikehara Y, Narimatsu H. Glycoproteomics approach for identifying Glycobiomarker candidate molecules for tissue type classification of non-small cell lung carcinoma. J Proteome Res. 2014. 13(11): 4705-16.

[59] Chen WJ, Ho CC, Chang YL, Chen HY, Lin CA, Ling TY, Yu SL, Yuan SS, Chen YJ, Lin CY, Pan SH, Chou HY, Chen YJ, Chang GC, Chu WC, Lee YM, Lee JY, Lee PJ, Li KC, Chen HW, Yang PC. Cancer-associated fibroblasts regulate the plasticity of lung cancer stemness via paracrine signalling. Nat Commun. 2014. 5: 3472.

[60] Lv G, Tan Y, Lv H, Fang T, Wang C, Li T, Yu Y, Hu C, Wen W, Wang H, Yang W. MXR7 facilitates liver cancer metastasis via epithelial-mesenchymal transition. Sci China Life Sci. 2017. 60(11): 1203-1213.

[61] Hebeiss I, Truckenmüller R, Giselbrecht S, Schepers U. Novel three-dimensional Boyden chamber system for studying transendothelial transport. Lab Chip. 2012. 12(4): 829-34.

[62] Olumi AF, Grossfeld GD, Hayward SW, Carroll PR, Tlsty TD, Cunha GR. Carcinoma-associated fibroblasts direct tumor progression of initiated human prostatic epithelium. Cancer Res. 1999. 59(19): 5002-11.

[63] Zhang Q, Liu T, Qin J. A microfluidic-based device for study of transendothelial invasion of tumor aggregates in realtime. Lab Chip. 2012. 12(16): 2837-42.

[64] Igarashi K, Murakami T, Kawaguchi K, Kiyuna T, Miyake K, Zhang Y, Nelson SD, Dry SM, Li Y, Yanagawa J, Russell TA, Singh AS, Tsuchiya H, Elliott I, Eilber FC, Hoffman RM. A patient-derived orthotopic xenograft (PDOX) mouse model of a cisplatinum-resistant osteosarcoma lung metastasis that was sensitive to temozolomide and trabectedin: implications for precision oncology. Oncotarget. 2017. 8(37): 62111-62119.

[65] Du H, Chen D, Zhou Y, Han Z, Che G. Fibroblast phenotypes in different lung diseases. J Cardiothorac Surg. 2014. 9: 147.

[66] Wang D, Fang M, Shen N, Li L, Wang W, Wang L, Lin H. Inhibiting post-translational core fucosylation protects against albumin-induced proximal tubular epithelial cell injury. Am J Transl Res. 2017. 9(10): 4415-4427.

[67] Pang X, Wang Y, Zhang S, Tan Z, Guo J, Guan F, Li X. Altered susceptibility to apoptosis and N-glycan profiles of hematopoietic KG1a cells following co-culture with bone marrow-derived stromal cells under hypoxic conditions. Oncol Rep. 2018. 40(3): 1477-1486.

[68] Okagawa Y, Takada K, Arihara Y, Kikuchi S, Osuga T, Nakamura H, Kamihara Y, Hayasaka N, Usami M, Murase K, Miyanishi K, Kobune M, Kato J. Activated p53 with Histone Deacetylase Inhibitor Enhances L-Fucose-Mediated Drug Delivery through Induction of Fucosyltransferase 8 Expression in Hepatocellular Carcinoma Cells. PLoS One. 2016. 11(12): e0168355.

[69] Wang X, Fukuda T, Li W, Gao CX, Kondo A, Matsumoto A, Miyoshi E, Taniguchi N, Gu J. Requirement of Fut8 for the expression of vascular endothelial growth factor receptor-2: a new mechanism for the emphysema-like changes observed in Fut8-deficient mice. J Biochem. 2009. 145(5): 643-51.

[70] Wang Z. ErbB Receptors and Cancer. Methods Mol Biol. 2017. 1652: 3-35.

[71] Azimzadeh Irani M, Kannan S, Verma C. Role of N-glycosylation in EGFR ectodomain ligand binding. Proteins. 2017. 85(8): 1529-1549.

Tables

Due to techinical limitations, Tables 1-4 available in the Supplementary Files section below.

Supplementary Figure Captions

Supplementary figure.1 (a) Comparison of FUT8 across the 7 analyses shows the detailed information of the 7 datasets. (b) Morphological characteristics were observed with an inverted microscope. Scale bar: 500 μm. (c) The schematic diagram and a real photo of the improved design of the coculture device used in the current study. A more detailed blueprint for 3D printing is available freely from the corresponding authors upon request. (e) Time-concentration curves were drawn by testing the concentration of the standard protein solution in the two wells with a BCA quantitative kit and a microplate reader. The experiment was repeated three times.

Supplementary figure.2 (a) Apoptosis of A549 and H322 cells cocultured with fibroblasts were tested by AO/EB staining assays. The experiments were repeated three times, and the quantitative data are shown in the bar chart. (b) Apoptosis of A549 and H322 cells cocultured with fibroblasts were tested by AV/PI staining and flow cytometry. Quantitative data are shown in the bar charts.

Supplementary figure.3 (a) KEGG analysis shows 20 biochemical functional domains that are significantly regulated by FUT8/CF activity in CAFs. (b) (c) (d) Heat map based on the folds of change in expression of genes in the three signaling pathways. Color from red to blue: gene expression in CAFs compared with the median level. Zoom in to see the gene names on the left side of the heat maps.

Figures

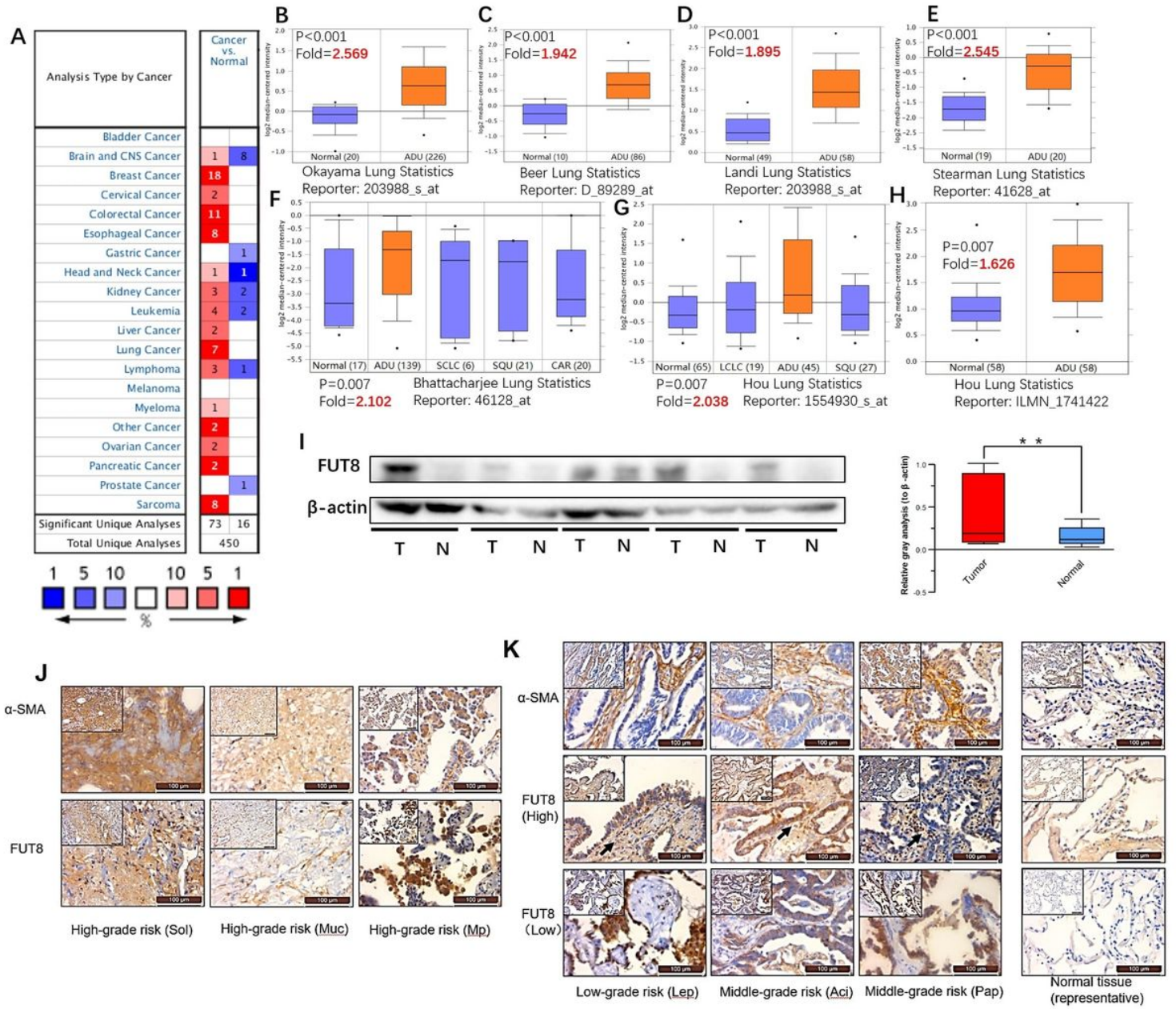

Figure 1

FUT8 was overexpressed in the CAFs of most adenocarcinoma cases. (a) Cancer type analysis of 89 datasets in Oncomine. Red: overexpression. Blue: low-expression. (b-h) Box charges showing the FUT8 levels across cancer/normal tissues. Sample size of each group is marked in brackets. ADU: lung adenocarcinoma. SCLC: small cell lung cancer. SQU: squamous cell lung carcinoma. CAR: lung carcinoid tumor. LCLC: large cell lung cancer. (i) FUT8 was tested by western blotting in 5 NSCLC and paired normal tissues. (j) Representative images of α-SMA and FUT8 tested by IHC in the 3 excluded histological subtypes of lung adenocarcinoma. (L) Representative images of α-SMA and FUT8 tested by IHC in lung adenocarcinomas and paired adjacent tissues. Sol: solid, Muc: mucinous, Mp: micropapillary, Lep: lepidic, Aci: acinar, Pap: papillary predominant adenocarcinoma. Scale bar: 100 μm.

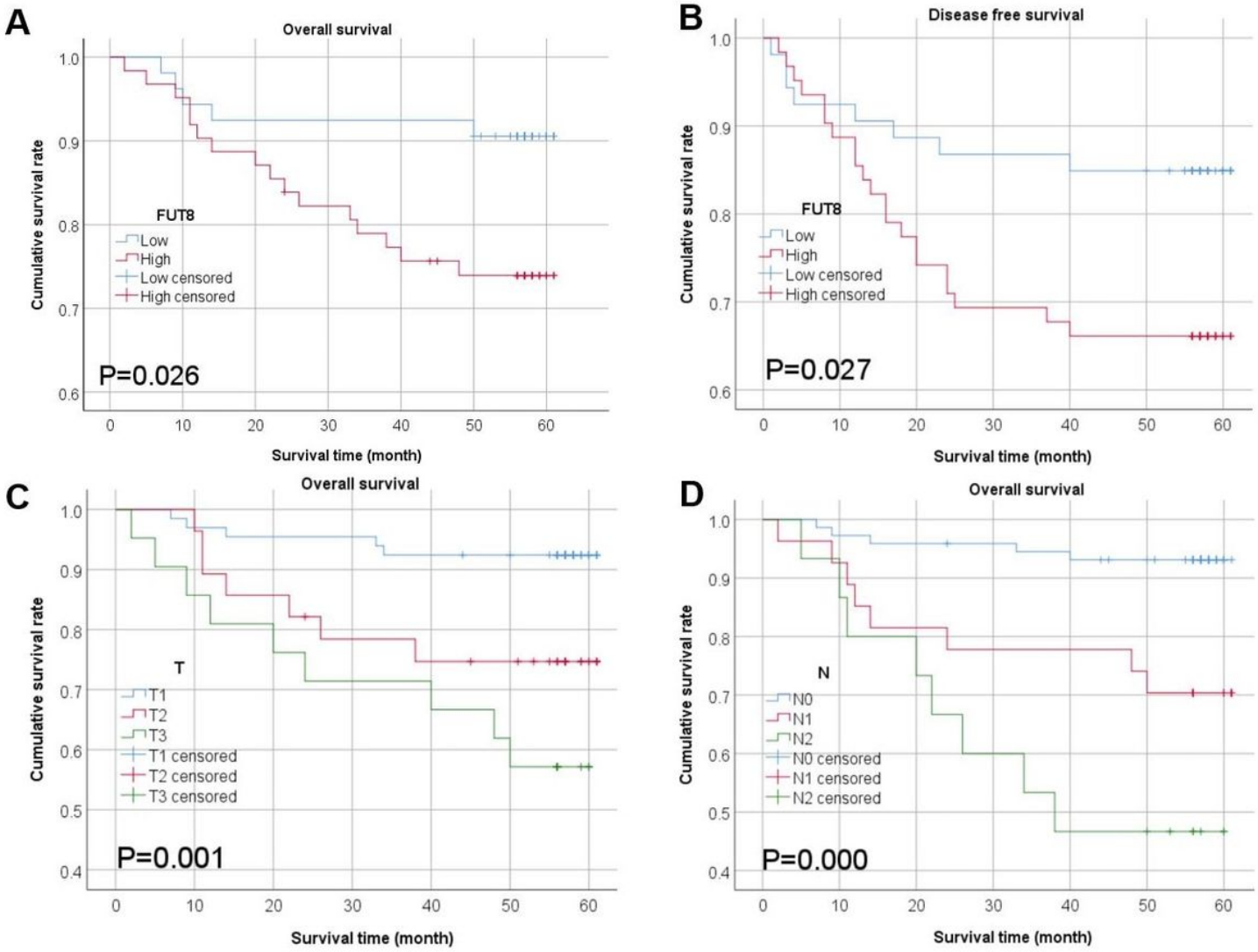

Figure 2

FUT8 expression in CAFs correlates with long-term prognosis. Survival curves are drawn by Kaplan-Miere survival analysis regarding the relationship between (a) FUT8 in CAFs and overall survival, (b) FUT8 in CAFs and disease-free survival, (c) T staging and overall survival, (d) N staging and overall survival. Censored data are marked with short lines perpendicular to the curves.

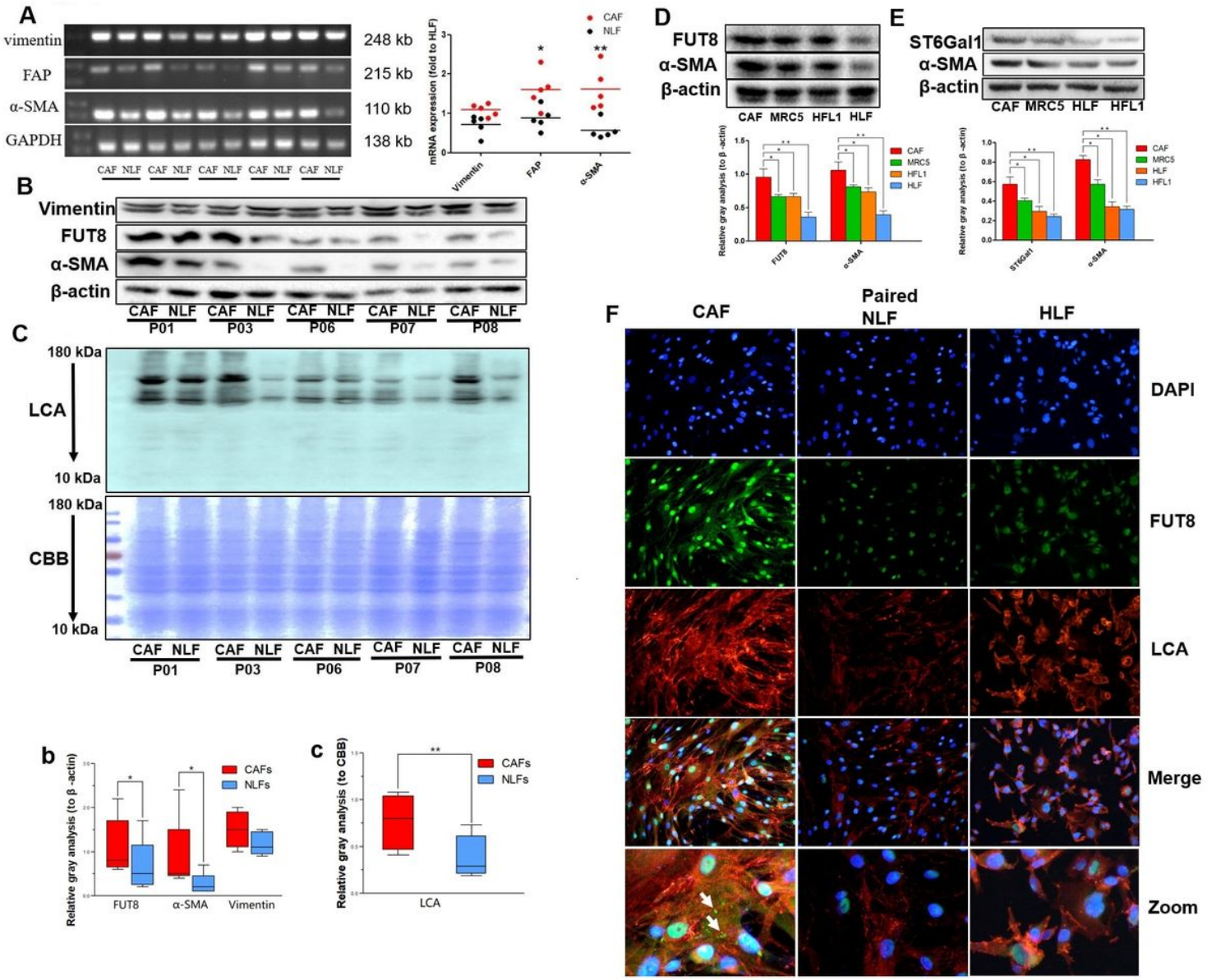

Figure 3

FUT8 is overexpressed in CAFs and mediates high levels of CF. (a) Myofibroblast markers in the total RNA of the 5 pairs of primary fibroblasts were tested by RT-PCR. Quantitative data are shown in the dot chart. (b) Myofibroblast markers and FUT8 were tested by western blotting in primary CAFs and paired NLFs. Quantitative data are shown in the box chart. (c) Corresponding fucosaccharide binding levels were tested by lection boltting. LCA: lens culinaris agglutinin. CBB: Coomassie brilliant blue. Quantitative data are shown in the box chart. (a) FUT8 and α-SMA were tested by western blotting in CAFs and lab-grown normal fibroblasts. Quantitative data are shown in the bar chart. (b) ST6Gal1 and α-SMA were tested by western blotting in CAFs and lab-grown normal fibroblasts. Quantitative data are shown in the bar chart. (f) FUT8 immunofluorescence (green) and fucosaccharide lectin fluorescence (red). White arrows: secretory vesicles containing large amounts of FUT8 were only observed in CAFs. Magnification: 400×/800×.

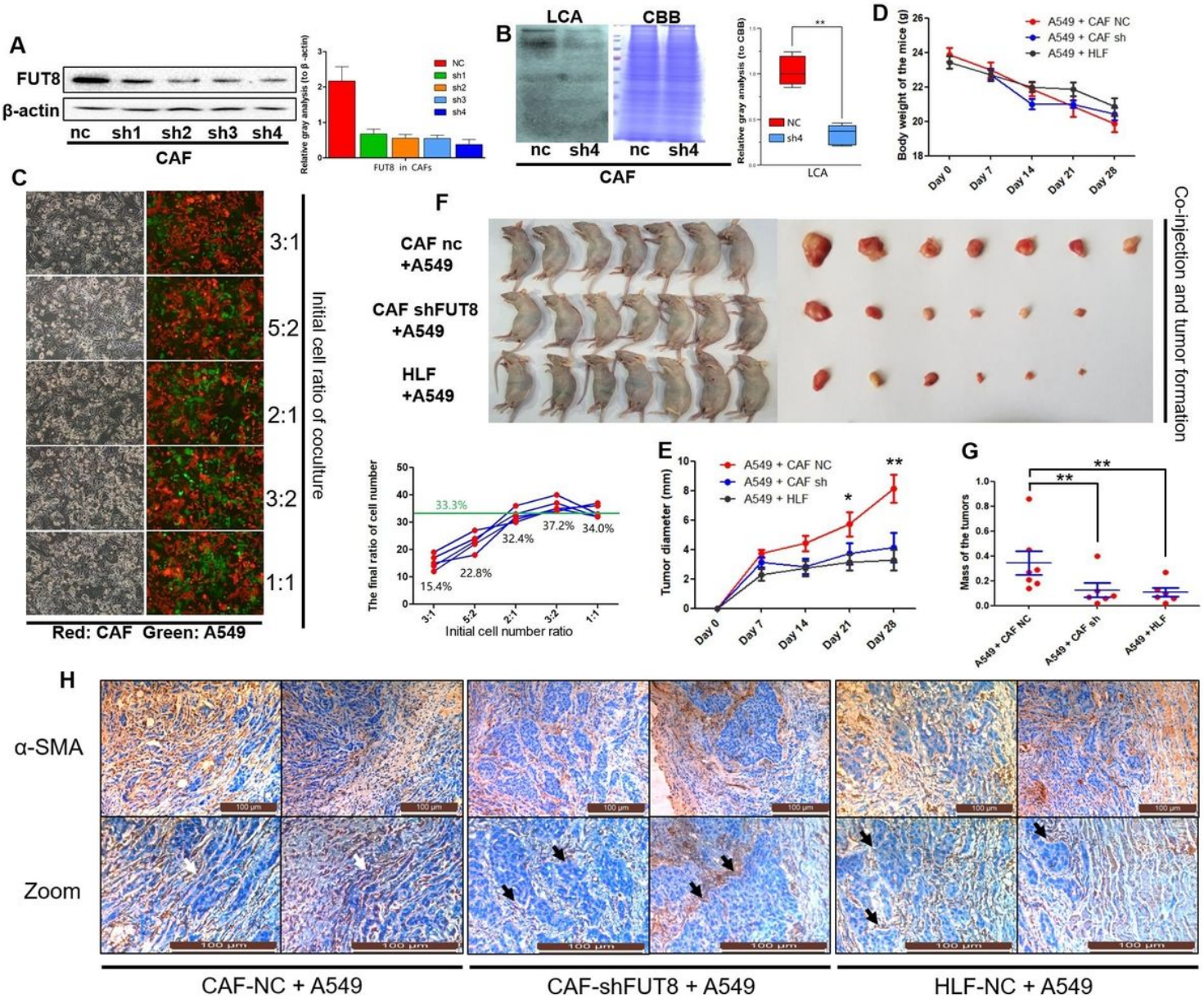

Figure 4

FUT8 in CAFs was necessary for the construction of an invasive tumor microenvironment in vivo. (a) 4 shRNA fragments were used for downregulating FUT8 in CAFs and the effects of gene intervention were tested by western blotting. Quantitative data are shown in the bar chart. (b) Lentivirus-packed sh4 was used to stably downregulate FUT8 in CAFs. The effects were tested lectin blotting. Quantitative data are shown in the box chart. (c) Fluorescent labeled A549 (green) and CAFs (red) were cocultured immediately and contiguously in vitro to stably mimics a TME similar to that of primary lung cancer. Magnification: 200×. Quantitative data are shown in the line chart. (d) Change in body weights of the mice are shown by line chart. (e) Changes in tumor diameters are shown by line chart. (f) Nude mice in the experiment and the generated tumors. (g) Wet weights of the tumors removed from the mice is shown by dot chart. (h) Histological structures of tumor stoma are marked with α-SMA IHC staining assays. In the CAF-shFUT8/A549 tumors and HLF/A549 tumors, the tumor cells preferred to clump together rather than

invade the stroma. white arrows: NSCLC cells invade into stromal cells. black arrows: The clear boundaries between tumor stroma and large masses of parenchyma. Scale bar: 100 μm.

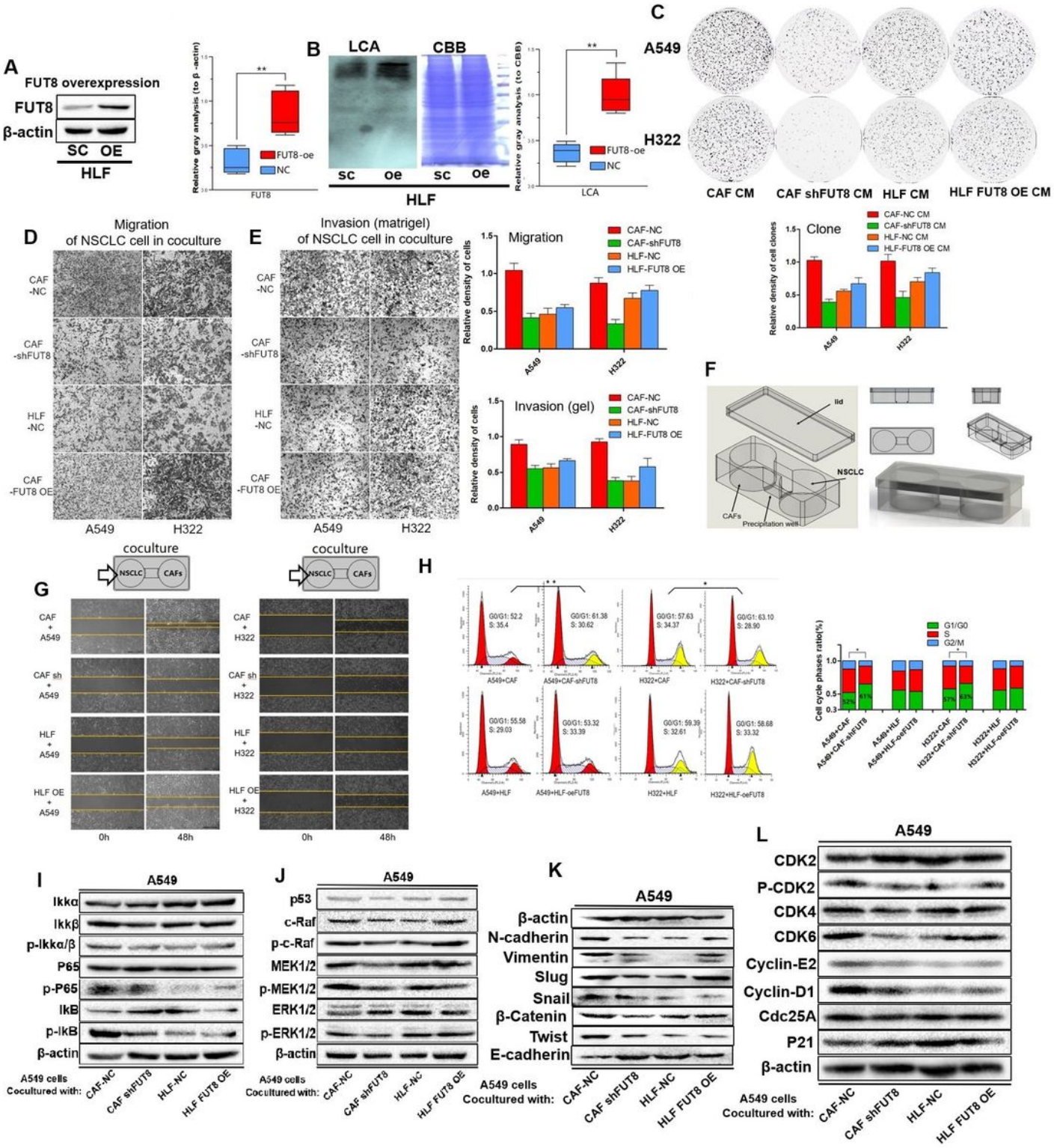

Figure 5

CF mediated by FUT8 is necessary for maintaining the protumorigenic capacity of CAFs. (a) (b) Lentivirus-packed FUT8 coding sequence was used to stably upregulate FUT8 in HLFs. The effects were tested by western blotting and lectin blotting. Quantitative data are shown in the box charts. (c)

Proliferation of A549 and H322 cells cultured with the conditioned medium of CAFs or HLFs were tested by clone formation assay. Quantitative data are shown in the bar chart. (d) (e) Migration and invasion (matrigel) of A549 and H322 cells cocultured with the fibroblasts were tested by Transwell assays. Magnification: 100×. Quantitative data are shown in the bar charts. (f) The schematic diagram of the device for the establishment of an in vitro non-contact coculture system. A more detailed blueprint for 3D printing is available freely from the corresponding authors upon request. (g) Migration of A549 and H322 cells cocultured with the fibroblasts in the non-contact coculture system were tested by wound healing assays. Magnification: 200×. All the experiments were repeated three times. (h) Cell cycle of A549 and H322 cells cocultured with the fibroblasts were tested by PI staining and flow cytometry. And the quantitative data are shown in the bar chart. Yellow peaks: diploids were observed in the assessed cells. Quantitative data are shown in the bar chart. (i) (j) (k) (l) Signaling pathways of NF-kB, MAPK/ERK1/2, Biomarkers of Mesenchymal epithelial transformation (EMT) and cell cycle G1/S checkpoint in A549 cells cocultured with fibroblasts in the non-contact coculture system were tested by western blotting. All experiments in this section were repeated three times.

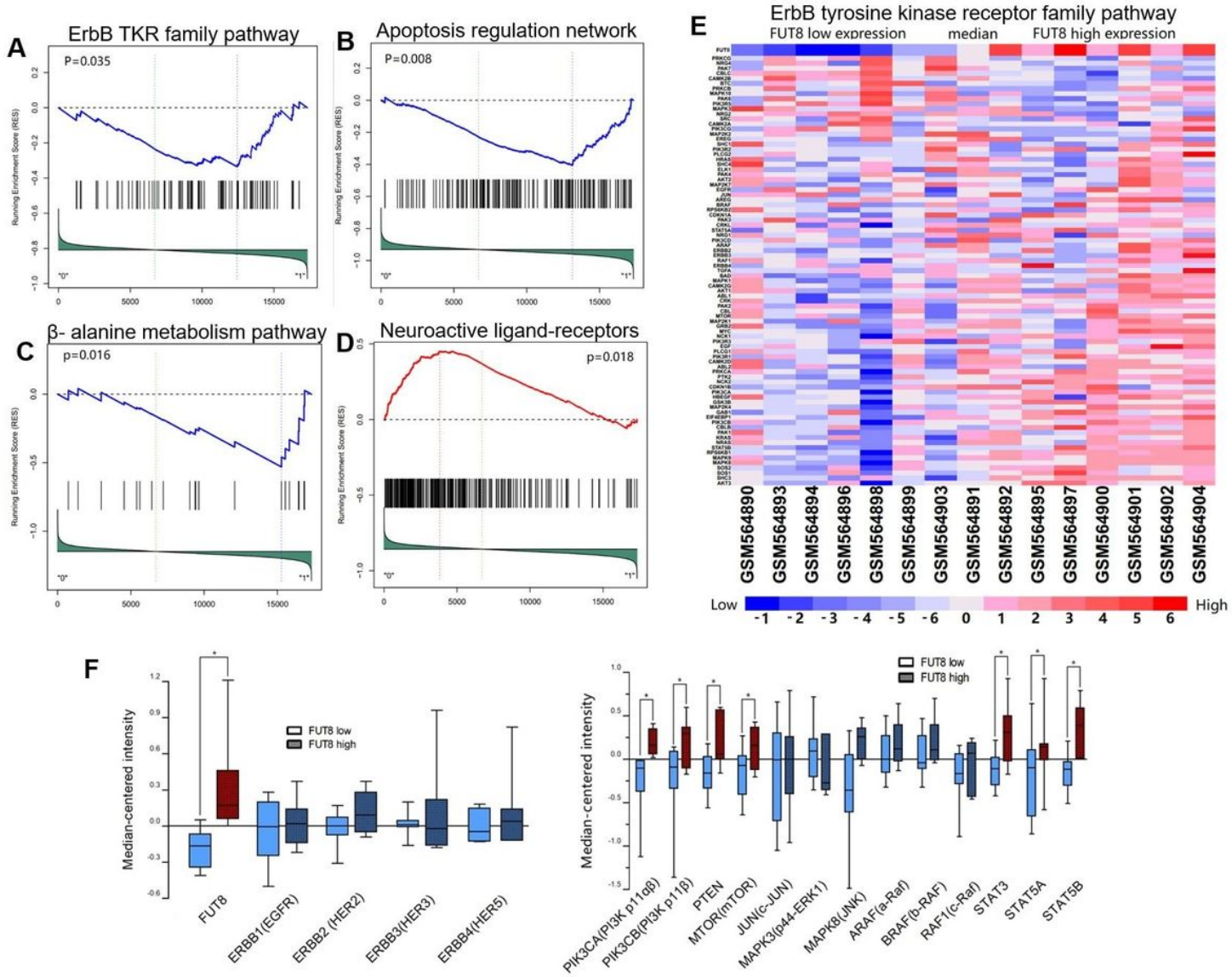

Figure 6

Potential mechanisms of FUT8 maintaining the tumor-promoting phenotype of CAFs. (a) (b) (c) (d) Gene set enrichment analysis (GSEA) shows the gene list index of the ErbB TKR family pathway, the apoptosis regulation network, the β-alanine metabolism pathway and the neuroactive ligand-receptors. TKR: tyrosine kinase receptor. (e) Heat map based on the folds of change in expression of genes in the ErbB tyrosine kinase receptor family pathway. Color from red to blue: gene expression in CAFs compared with the median level. Zoom in to see the gene names on the left side of the heat maps. (g) The expression of the ErbB genes in FUT8 high/low groups is shown by the box chart. (h) The expression of downstream genes of the ErbB signaling in FUT8 high/low groups is shown by the box chart.

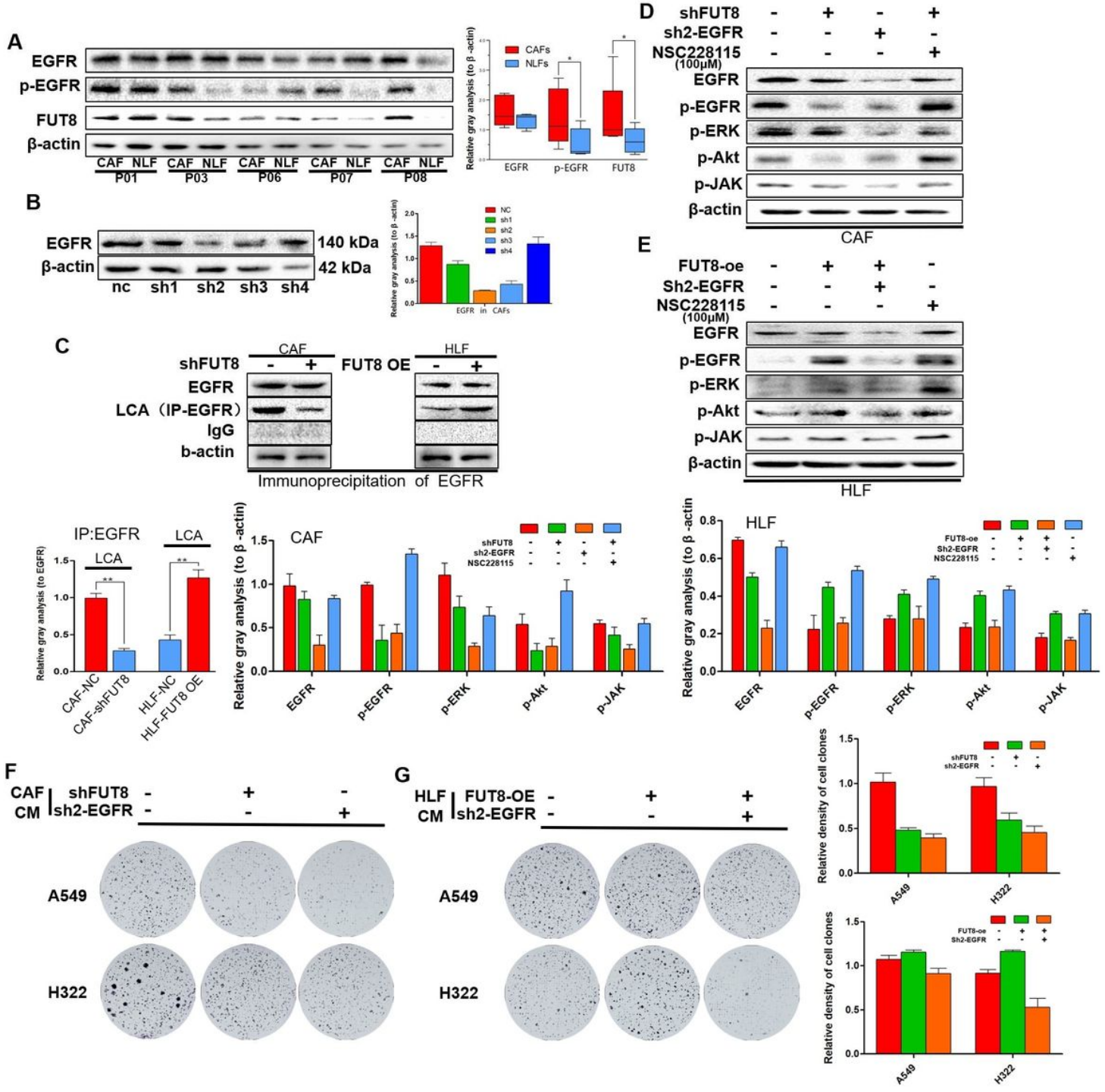

Figure 7

CF mediated by FUT8 regulates cancer-promoting capacities of CAFs via the modification of EGFR fucosylation. (a) EGFR, p-EGFR and FUT8 were tested by western blotting in primary CAFs and paired NLFs. Quantitative data are shown in the box chart. (b) 4 shRNA fragments were used for downregulating FUT8 in CAFs and the effects of gene intervention were tested by western blotting. Quantitative data are shown in the bar chart. (c) The binding of fucose to EGFR was tested by immunoprecipitation (IP) and lectin blotting. Quantitative data are shown in the bar chart. (d)(e) EGFR signaling and the phosphorylation of ERK, JAK and Akt in CAFs and HLFs were tested by western blotting. Quantitative data are shown in the bar charts. NSC 228155 is an activator of EGFR, binds to the extracellular region of EGFR and enhance tyrosine phosphorylation of EGFR. (f)(g) Proliferation of A549 and H322 cells cultured with the conditioned medium of CAFs or HLFs were tested by clone formation assay. Quantitative data are shown in the bar chart.

Supplementary Files

This is a list of supplementary files associated with this preprint. Click to download.

- Tables14.zip
- SupplementaryFilesSupplementaryFigures13.zip